

# Simple and Accurate Uncertainty Quantification from Bias-Variance Decomposition

Shi Hu<sup>1</sup> Nicola Pezzotti<sup>2</sup> Dimitrios Mavroeidis<sup>2</sup> Max Welling<sup>1</sup>

## Abstract

Accurate uncertainty quantification is crucial for many applications where decisions are in play. Examples include medical diagnosis and self-driving vehicles. We propose a new method that is based directly on the bias-variance decomposition, where the parameter uncertainty is given by the variance of an ensemble divided by the number of members in the ensemble, and the aleatoric uncertainty plus the squared bias is estimated by training a separate model that is regressed directly on the errors of the predictor. We demonstrate that this simple sequential procedure provides much more accurate uncertainty estimates than the current state-of-the-art on two MRI reconstruction tasks.

## 1. Introduction

With the rapid developments of artificial intelligence technology, many areas in our society begin to use AI to assist humans for decision making (Witherspoon & Fadrhanc, 2019). In general, AI methods are known to work well when trained with a large amount of data (Rajpurkar et al., 2017; Esteva et al., 2017), but can still make mistakes when tested on new data. On tasks that are related to human safety, such as computer-aided diagnosis or autonomous driving, it is especially important to accurately estimate the uncertainty in the model predictions.

The uncertainty can be classified into two categories: epistemic and aleatoric. According to (Kureghian & Ditlevsen, 2007), the epistemic uncertainty is reducible by gathering more data or by refining models. On the other hand, the aleatoric uncertainty cannot be reduced. (Kendall & Gal, 2017) uses this definition to quantify uncertainties in computer vision tasks, where they model the aleatoric as the heteroscedastic label noise, and the epistemic as the randomness in the model parameters. However, the model bias,

which can be reduced if we have more knowledge in the structure of the underlying model, seems to be missing from the epistemic uncertainty quantification.

(Kennedy & O’Hagan, 2001) provides a more fine-grained categorization of uncertainty into six terms. Among them, the parameter and experimental uncertainties correspond to the epistemic and aleatoric uncertainties in (Kendall & Gal, 2017), and the structural uncertainty corresponds to the missing model bias. For clarity, from now on we switch to the uncertainty terminologies defined in (Kennedy & O’Hagan, 2001) for the rest of this paper.

We model the three aforementioned uncertainties from (Kennedy & O’Hagan, 2001) using the bias-variance decomposition, where the squared bias, noise and variance terms from the decomposition correspond to the structural, experimental and parameter uncertainties respectively.

We first apply our method to a toy example and show that by squeezing out the structural uncertainty from the total, the experimental uncertainty can be more accurately measured. We then apply our method to two MRI reconstruction tasks in the fastMRI challenge<sup>1</sup>, and show that we achieve the state-of-the-art uncertainty quantification results.

The contributions of this paper are:

- Novel uncertainty decomposition for deep ensembles with parameter uncertainty inversely scaled by the number of ensemble members.
- Two-stage process for target and uncertainty estimations that significantly reduces the bias and improves uncertainty prediction results compared to the current state-of-the-art.
- Strong adaptability to both simple and complex models, easy to implement and requires no modification to the model.
- Clarification of the uncertainty quantification terminologies used in the machine learning and computer vision communities.

<sup>1</sup>University of Amsterdam <sup>2</sup>Philips Research. Correspondence to: Shi Hu <s.hu@uva.nl>.

<sup>1</sup><https://fastmri.org/>

## 2. Related Works

In the following text, we denote  $x$  as the input data,  $y(x)$  the noisy label,  $h(x)$  the true label and  $\epsilon(x)$  the label noise.

(Gal & Ghahramani, 2016) is a Bayesian method that quantifies the predictive uncertainty by adding dropout (Srivastava et al., 2014) to the neural networks. For each input  $x$ , they run the network  $T$  times to produce  $T$  Monte Carlo predictions  $\hat{y}_t(x)$ 's. Their final prediction is  $\mathbb{E}[\hat{y}_t(x)]$  and the predictive uncertainty is  $\text{Var}[\hat{y}_t(x)] + \text{const.}$

Many estimation problems can be written in the form of:

$$y(x) = h(x) + \epsilon(x), \quad (1)$$

with the heteroscedastic noise  $\epsilon(x) \sim \mathcal{N}(0, \sigma^2(x))$ . (Nix & Weigend, 1994) introduced a method to estimate both  $h(x)$  and  $\sigma^2(x)$  simultaneously by splitting the last layer of a neural work into two branches  $[\hat{y}(x), \hat{\sigma}^2(x)]$  and minimizing the negative Gaussian log-likelihood:  $\frac{1}{2} \frac{\|y(x) - \hat{y}(x)\|^2}{\hat{\sigma}^2(x)} + \frac{1}{2} \log \hat{\sigma}^2(x)$ .

(Kendall & Gal, 2017; Tanno et al., 2017) extended this idea by adding dropout to the neural network to produce  $T$  Monte Carlo estimates  $[\hat{y}_t(x), \hat{\sigma}_t^2(x)]_{t=1 \dots T}$ , where each estimate  $[\hat{y}_t(x), \hat{\sigma}_t^2(x)]$  parameterizes a Gaussian distribution. Thus, the  $T$  samples parameterize a Gaussian mixture distribution, whose mean is  $\frac{1}{T} \sum_t \hat{y}_t(x)$  and total variance is  $\mathbb{E}_t[\hat{\sigma}_t^2(x)] + \text{Var}_t[\hat{y}_t(x)]$ . The two terms in the total variance are the experimental and parameter uncertainties respectively. The experimental models the variance  $\sigma^2(x)$  of the label noise distribution, and the parameter models the randomness of the model parameters.

Both (Nix & Weigend, 1994) and (Kendall & Gal, 2017) estimate the experimental uncertainty using the learned loss attenuation from the Gaussian log-likelihood loss. When there are multiple annotations per image, (Hu et al., 2019) proposed to explicitly model the experimental uncertainty based on the Probabilistic U-net (Kohl et al., 2018) by treating the inter-grader variability as the target in supervised learning.

(Lakshminarayanan et al., 2017) proposed a non-Bayesian method to estimate the predictive uncertainty using deep ensembles. Following (Nix & Weigend, 1994), they split the last layer of each ensemble network into two branches  $[\hat{y}(x), \hat{\sigma}^2(y)]$ , and train the network using a proper scoring rule as the Gaussian log-likelihood. The outputs from the deep ensemble models parameterize a Gaussian mixture distribution, whose mean and total variance have the same form as in (Kendall & Gal, 2017). However, instead of decomposing the total variance into experimental and parameter, they approximate the Gaussian mixture distribution with a

single Gaussian of the same mean and variance, where the variance is used as the predictive uncertainty. They also show that the predictive uncertainty can be improved using adversarial training (Goodfellow et al., 2015).

(Zhu & Laptev, 2017) proposed to decompose the prediction uncertainty from Bayesian neural networks into model uncertainty, homoscedastic inherent noise and model misspecification. They estimate the sum of the model uncertainty and model misspecification using the variance of samples from the Monte Carlo dropout, and homoscedastic inherent noise by computing the variance of an independent validation set under the assumptions that their predictor is unbiased and their training set is very large.

## 3. Method

Following the notations in Section 2, the mean squared error for any model prediction  $\hat{y}(x)$  is  $\mathbb{E}_{\epsilon, \hat{y}(x)}[(y(x) - \hat{y}(x))^2]$ , which can be decomposed into bias<sup>2</sup>, noise and variance from the bias-variance decomposition as follows:

$$\mathbb{E}_{\epsilon, \hat{y}(x)}[(y(x) - \hat{y}(x))^2] \quad (2)$$

$$= (h(x) - \mathbb{E}_{\hat{y}(x)}[\hat{y}(x)])^2 + \mathbb{E}_{\epsilon(x)}[\epsilon^2(x)] \quad (3)$$

$$+ \mathbb{E}_{\hat{y}(x)}[(\mathbb{E}_{\hat{y}(x)}[\hat{y}(x)] - \hat{y}(x))^2] \quad (4)$$

$$= \text{bias}[\hat{y}(x)]^2 + \sigma^2(x) + \text{Var}[\hat{y}(x)].$$

For (Kendall & Gal, 2017),  $\hat{y}(x)$  represents a target prediction from one MC dropout sample, so the mean of the MC target predictions model  $\mathbb{E}_{\hat{y}(x)}[\hat{y}(x)]$ . Further, the experimental and parameter uncertainties model  $\sigma^2(x)$  and  $\text{Var}[\hat{y}(x)]$  in Eq. 4 respectively.

### 3.1. Uncertainty Decomposition for Deep Ensembles

We estimate the parameter uncertainty by training a “deep ensemble” (see e.g. (Lakshminarayanan et al., 2017)). We train an ensemble of  $K$  members where each member predicts the target label. The mean of this ensemble is:

$$\hat{\mu}(x) = \frac{1}{K} \sum_{k=1}^K \hat{y}_k(x) \quad (5)$$

is used as the estimator for  $\mathbb{E}_{\hat{y}(x)}[\hat{y}(x)]$ . Assuming the ensemble members are i.i.d., applying the same bias-variance decomposition to  $\hat{\mu}(x)$  gives:

$$\mathbb{E}_{\epsilon, \hat{\mu}(x)}[(y(x) - \hat{\mu}(x))^2] \quad (6)$$

$$= \text{bias}[\hat{\mu}(x)]^2 + \sigma^2(x) + \text{Var}_{\hat{\mu}(x)}[\hat{\mu}(x)] \quad (7)$$

$$= \text{bias}[\hat{y}(x)]^2 + \sigma^2(x) + \frac{1}{K} \text{Var}_{\hat{y}(x)}[\hat{y}(x)]. \quad (8)$$

The parameter uncertainty is now provided by the variance of  $\hat{\mu}(x)$ , which is equal to  $\frac{1}{K} \text{Var}[\hat{y}(x)]$  where  $\text{Var}[\hat{y}(x)]$  represents the variance of the ensemble itself and  $K$  is the number of members in the ensemble. The factor  $1/K$  seems to be missed in earlier works.

In addition, we use

$$\hat{\nu}(x) = \frac{1}{K^2} \sum_{k=1}^K (\hat{y}_k(x) - \hat{\mu}(x))^2 \quad (9)$$

as an estimator for the variance of the mean estimators of the ensemble:  $\text{Var}_{\hat{\mu}(x)}[\hat{\mu}(x)] = \frac{1}{K} \text{Var}_{\hat{y}(x)}[\hat{y}(x)]$ .

### 3.2. Two-stage Target and Uncertainty Estimations

The structural or the experimental uncertainty cannot be estimated directly as we do not have access to the true function  $h(x)$  or the label noise  $\epsilon(x)$  individually. However, their sum is the difference between the expected error of the mean estimator and its variance:

$$\text{bias}[\hat{y}(x)]^2 + \sigma^2(x) \quad (10)$$

$$= \mathbb{E}_{\epsilon, \hat{\mu}(x)}[(y(x) - \hat{\mu}(x))^2] - \frac{1}{K} \text{Var}[\hat{y}(x)]. \quad (11)$$

Given a noisy label and an ensemble estimator, both terms in Eq. 11 are accessible for  $K \geq 2$ .

To estimate the prediction uncertainty for  $\hat{\mu}(x)$ , we use a neural network  $U$  to learn the uncertainty distribution at  $x$  by regressing the uncertainty prediction  $U(x)$  to the squared errors  $(y(x) - \hat{\mu}(x))^2$ .

The above two-stage process can be used to solve the estimation problem of Eq. 1 as follows: we first train  $\hat{\mu}(x)$  to predict  $h(x)$  from the noisy label  $y(x)$ , then train  $U(x)$  to predict the squared error of  $\hat{\mu}(x)$ . The target for  $U(x)$  subtracted by  $\frac{1}{K} \text{Var}[\hat{y}(x)]$  approaches the experimental uncertainty when the bias of  $\hat{\mu}(x)$  decreases. Furthermore, the complexity of each network depends on their task. For problems where the true function has complex patterns but the label noise has simpler patterns, a simpler network for  $U(x)$  can be used to predict the errors for the complex task.

We note that this is in sharp contrast to (Nix & Weigend, 1994; Kendall & Gal, 2017) which train one (torso) network to the data with two heads: one for the prediction  $\hat{y}(x)$  and one for the standard deviation  $\hat{\sigma}^2(x)$ . We argue that since  $h(x)$  and  $\sigma^2(x)$  are independent quantities, joint estimation would lead to interference between these objectives. We demonstrate that our method can achieve significant bias reduction as well as higher experimental uncertainty prediction accuracy in Section 4.1.

### 3.3. Efficient Inference via Distillation

For efficient inference, we train single networks  $D_\mu(x)$  and  $D_\nu(x)$  to approximate  $\hat{\mu}(x)$  and  $\hat{\nu}(x)$  respectively using distillation (Hinton et al., 2015).

In sum, we propose a sequential procedure that first estimates the target label as the mean prediction of an ensemble. Parameter uncertainty is now given by  $1/K$  times the variance of the predictions made by the ensemble. We then fit a network  $U$  to the prediction errors made by the ensemble mean. We call this the predictive ensemble which contains structural, experimental and parameter uncertainty. Thus subtracting the estimated parameter uncertainty from this quantity, we are left with the sum of the structural and the experimental uncertainties. This quantity is close to the experimental (irreducible, aleatoric) uncertainty if we assume that the bias in our model is small (i.e. if we use highly flexible models in our ensemble).

## 4. Experiments

We demonstrate our method on two tasks: curve fitting and MRI reconstruction. Curve fitting is a toy example where the synthetic true function and noise distribution are known. MRI reconstruction is a large scale experiment using real-world data.

### 4.1. Curve Fitting

We use the same synthetic example shown in Section B.1 of (Nix & Weigend, 1994): given a noisy label  $y(x) = f(x) + \epsilon(x)$ ,  $\epsilon(x) \sim \mathcal{N}(0, \sigma^2(x))$ , we want to estimate the true underlying function  $f(x)$  and the noise variance  $\sigma^2(x)$  for  $x \in [0, \pi/2]$ , which are:

$$f(x) = \sin(4x) \sin(5x) \quad (12)$$

$$\sigma^2(x) = 0.02 + 0.02 \times [1 - \sin(4x)]^2. \quad (13)$$

To create the synthetic training set, in each epoch we randomly sample 1000 points in the interval  $[0, \pi/2]$ . For each point  $x$ , we sample the noise  $\epsilon(x)$  from its distribution  $\mathcal{N}(0, \sigma^2(x))$   $R$  times. Each noise sample  $\epsilon_r(x)$  is then added to the true function  $f(x)$  to produce a noisy label  $y_r(x)$ . This procedure creates  $R$  noisy labels per  $x$ .

We use a simple neural network with one hidden layer of 100 units with ReLU non-linearities (Nair & Hinton, 2010), and optimize using the Adam optimizer (Kingma & Ba, 2015) with learning rate  $10^{-5}$  suggested by (Nix & Weigend, 1994). We train the network for 10000 epochs.

For (Kendall & Gal, 2017), we additionally use dropout with dropout rate 0.2 after ReLU, and split the last layer into the mean prediction  $\hat{y}(x)$  and the log variance  $s(x) =$

$\log \hat{\sigma}^2(x)$ . Since we are predicting two outputs simultaneously, we use 200 hidden units in the network for fairness. We train with the negative Gaussian log-likelihood loss with  $R$  labels per  $x$ :

$$\frac{1}{2} \exp(-s(x)) \frac{\sum_r \|y_r(x) - \hat{y}(x)\|^2}{R} + \frac{1}{2} s(x) \quad (14)$$

$$= \frac{1}{2} \exp(-s(x)) \left[ (h(x) - \hat{y}(x))^2 + \frac{\sum_r \epsilon_r^2 + 2 \sum_r \epsilon_r (h(x) - \hat{y}(x))}{R} \right] + \frac{1}{2} s(x). \quad (15)$$

During testing, we draw 50 MC dropout samples  $[\hat{y}_t(x), \hat{\sigma}_t^2(x)]$  to produce the final prediction  $\frac{1}{T} \sum_t \hat{y}_t(x)$  and the experimental uncertainty  $\frac{1}{T} \sum_t \hat{\sigma}_t^2(x)$ .

From Eq. 14, we can show the optimal value for  $\hat{\sigma}^2(x)$  is:

$$\text{bias}[\hat{y}(x)]^2 + \frac{\sum_r \epsilon_r^2 + 2 \sum_r \epsilon_r (h(x) - \hat{y}(x))}{R}. \quad (16)$$

This means the optimal  $\hat{\sigma}^2(x)$  converges to  $\text{bias}[\hat{y}(x)]^2 + \sigma^2(x)$  as  $R \rightarrow \infty$ . Figure 1 shows the experimental uncertainty predictions  $\hat{\sigma}^2(x)$  when we increase  $R$  from 1 to 100. In each plot, “K & G” is the result from the original method, and “K & G (no bias)” is the result if we replace the predictor  $\hat{y}(x)$  with the true function  $h(x)$  in Eq. 14. These plots show that  $\hat{\sigma}^2(x)$  in the original method do not converge to  $\sigma^2(x)$  due to the existence of significant bias.

Based on this observation, we argue that the key to improve the experimental uncertainty prediction is to reduce the bias. Since the true function  $h(x)$  and the experimental uncertainty  $\sigma^2(x)$  are independent quantities, we propose to estimate them sequentially as follows: we first train a network  $\text{Net}_h$  to regress on the true function  $h(x)$  from the based on noisy labels  $y(x)$ . Once  $\text{Net}_h$  is trained, we fix its weights and train a second network  $\text{Net}_s$  to regress on  $\sigma^2(x)$  from the squared residual  $\|y(x) - \hat{y}(x)\|^2$ , where  $\hat{y}(x)$  is predicted by  $\text{Net}_h$ .

To be comparable with Eq. 14, we use the MSE loss for the first step. For the second step, since we use a single predictor  $\hat{y}(x)$  in this example, we ignore the ensemble variance term in Eq. 11. Then, as each noise  $\epsilon_r(x)$  follows a Gaussian distribution  $\mathcal{N}(0, \sigma^2(x))$ , when the bias is small, the squared residual is approximately  $\epsilon_r^2(x)$ . This means that  $\frac{\|y_r(x) - \hat{y}(x)\|^2}{\sigma^2(x)}$  roughly follows a  $\chi_1^2$  distribution, and maximizing its log-likelihood with respect to  $\sigma^2(x)$  gives the same loss as in Eq. 14.

In general, the losses for the two steps depend on the distributions of the true function and the label noise. A benefit of

our method is the flexibility to choose each one separately as the two losses are decoupled.

We repeat each experiment 100 times, and plot the mean absolute errors (mean  $\pm$  std. error) for the biases and experimental uncertainty predictions in Figure 2. These results show our method can significantly reduce the bias and increase the experimental uncertainty prediction accuracy.

## 4.2. MRI Reconstruction

Our task is to reconstruct the fully-sampled MRIs and estimate the reconstruction uncertainty from the 4- and 8-fold accelerated under-sampled k-space data.

### 4.2.1. DATASETS

The NYU fastMRI dataset is the first large-scale release of the raw MRI data, which currently contains knee and brain MRIs (Zbontar et al., 2018). The knee dataset contains both single- and multi-coil MRIs. We use the multi-coil one as it is more clinically relevant (Zbontar et al., 2018). The brain dataset contains T1 weighted, T2 weighted and FLAIR multi-coil images, and we use the FLAIR subset. Table 1 shows the details about each dataset.

| Knee        |         |        |            |
|-------------|---------|--------|------------|
|             | Volumes | Slices | Sizes (GB) |
| train       | 973     | 34742  | 931        |
| validation  | 199     | 7135   | 192        |
| FLAIR Brain |         |        |            |
|             | Volumes | Slices | Sizes (GB) |
| train       | 344     | 5456   | 119        |
| validation  | 107     | 1694   | 38         |

Table 1. fastMRI datasets.

### 4.2.2. EXPERIMENTAL DETAILS

We train our estimators  $\hat{\mu}(x)$  and  $\hat{\nu}(x)$  using a similar method as in (Lakshminarayanan et al., 2017), which is to train an ensemble of  $K = 5$  models, where each uses the entire training set with a different initialization. We train the network  $U(x)$  to predict the absolute error  $|y(x) - \hat{\mu}(x)|$  using the normalized MSE (NMSE) loss<sup>2</sup>. Further, we train the distilled networks  $D_\mu(x)$  and  $D_\nu(x)$  using the  $\mathcal{L}_1$  and NMSE losses respectively.

We use two current state-of-the-art methods as baselines: the MC dropout (Gal & Ghahramani, 2016) with dropout rate 0.1 and 0.2, and the deep ensemble (Lakshminarayanan et al., 2017) with and without the adversarial training. Each method represents the predictive uncertainty using the model variance.

<sup>2</sup> $U(x)$  outputs the log of the squared error.

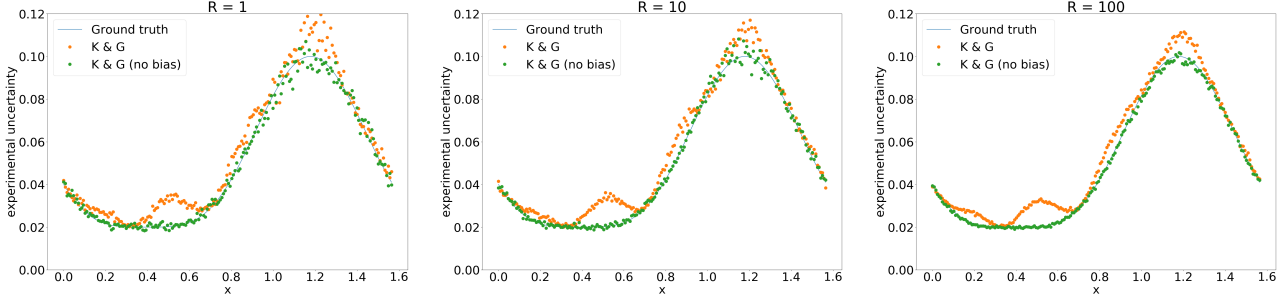


Figure 1. Experimental uncertainty predictions by (Kendall & Gal, 2017) versus the optimal.

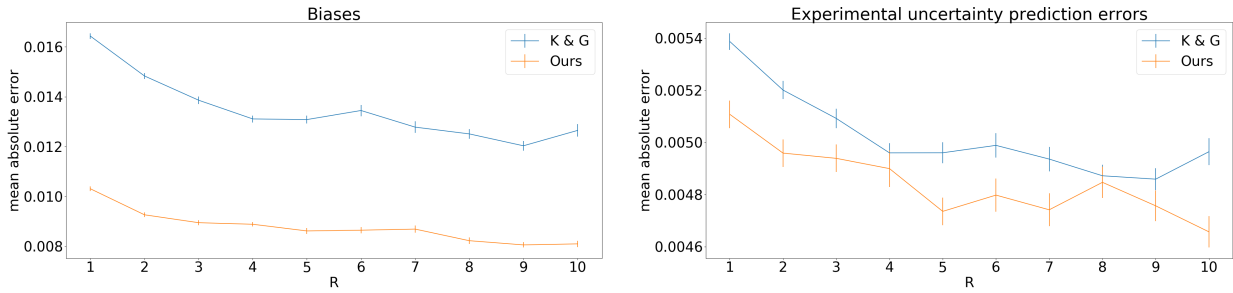


Figure 2. Comparison of the biases and experimental uncertainty prediction errors.

To measure the prediction error, we use the absolute error between the true target and a model’s reconstruction. Since all predictive uncertainties are in the squared image space, we compare the square root of each to their true prediction error.

Each baseline predictive uncertainty may have a different scale than their true prediction error. Thus, to be fair, we calibrate their uncertainty using 10-fold cross validation. In each iteration, we use one fold as the test set and the remaining as the training set. We perform the following optimization step on the training set:  $\min_{\alpha} \sum_i (d_i - \alpha u_i)^2$ , where  $i$  is the pixel index,  $d$  the true absolute error and  $u$  the predictive uncertainty. We then multiply the optimal  $\alpha$  to the predictive uncertainties in the test set for calibration. The optimal value for  $\alpha$  can be computed analytically as  $\sum_i d_i u_i / \sum_i u_i^2$ .

FastMRI’s train and validation sets provide fully-sampled k-space data, but the test set does not. Since the fully-sampled k-space data are required to evaluate the prediction error estimates, we train all methods on the training set and report results on the validation set.

An U-net (Ronneberger et al., 2015) implementation was provided by Facebook as the baseline for the fastMRI chal-

lenge<sup>3</sup>. It uses a weighted zero-filled image as input and trains with the  $\mathcal{L}_1$  loss.

The winning solution<sup>4</sup> in both 4- and 8-fold multi-coil tracks of the challenge is the Adaptive-CS-Net by Pezzotti et al. (Pezzotti et al., 2019). It uses the uncropped k-space data as input and trains with a weighted sum of Multiscale-SSIM and  $\mathcal{L}_1$  loss. We implement a smaller version of their model without the fine-tuning step. Training a single model takes 3 days on 2 Nvidia GV100 GPUs.

For ease of comparison, we implement all methods based on the U-net and use the same training procedure provided by the challenge: we train 40 epochs with the initial learning rate 0.001, then multiply the learning rate by 0.1 and train for an additional 10 epochs. We use 64 as the initial number of channels, and do not use dropout (except for MC dropout) or weight decay. The official implementation uses the validation set during training for model selection, but since we treat the validation set as our test set, we use the model at the end of training as the final model. Further, it uses the RMSProp optimizer (Tieleman & Hinton, 2012),

<sup>3</sup><https://github.com/facebookresearch/fastMRI>

<sup>4</sup><https://ai.facebook.com/blog/results-of-the-first-fastmri-image-reconstruction-challenge>



which we replace with Adam (Kingma & Ba, 2015).

To demonstrate the adaptability of our method, we report the results of our method on both the U-net and the Adaptive-CS-Net.

In sum, all U-net based methods have the same number of parameters, except for the deep ensemble, which uses twice the number of parameters as it has a two-head prediction architecture. Table 2 reports the number of model parameters for all methods in descending order.

| Method                   | #Params |
|--------------------------|---------|
| Deep Ensemble (+ AT)     | 27.66 M |
| MC Dropout (p=0.1 / 0.2) | 13.39 M |
| Ours (U-net)             | 13.39 M |
| Ours (Adaptive-CS-Net)   | 11.35 M |

Table 2. Number of model parameters.

#### 4.2.3. RESULTS

Table 3 and 4 ( $\mu \pm \sigma$ ) show the reconstruction and uncertainty prediction accuracy using the U-net and Adaptive-CS-Net on the two fastMRI multi-coil datasets. We divide all U-net based methods into two sections based on the number of models used for target predictions. For MC dropout (p=0.1 / 0.2) and our distillation methods, there is only one model to make predictions, and therefore their results will be less accurate than the ensemble-based methods in the other section, which are the deep ensemble (+ AT) and our full method.

For MRI reconstructions, we report the results using NMSE, PSNR and SSIM metrics following (Zbontar et al., 2018). For uncertainty predictions, we use both the absolute error metrics  $\mathcal{L}_1$  and MSE as well as the relative error metric NMSE. Also following (Zbontar et al., 2018), we highlight the best mean prediction result in each category.

We achieve good performance in MRI reconstructions, where we have the best results in 6/12 categories on the knee, and 10/12 on the FLAIR brain datasets. For uncertainty predictions, we have 10/12 best results on the knee, and 7/12 best results on the FLAIR brain datasets. In particular, we beat all baseline methods on the relative error metric by large margins.

For Adaptive-CS-Net, we achieve much stronger reconstruction results than all U-net based models despite having the smallest number of model parameters. For uncertainty predictions, Table 4 shows using the Adaptive-CS-Net to predict its ensemble mean error or distillation error is much more effective than using U-net.

Lastly, Figure 3 shows an example of a random knee MRI from the validation set and different types of uncertainties. We reconstruct the target using an ensemble from the 8-fold

accelerated k-space data. The true total error is the squared difference between the target and the ensemble mean. Since the true total error is noisy, we apply a Gaussian filter for smoothing. Our predicted total error is the third image, and the parameter uncertainty the fourth. The last image is the difference between the predicted total error and the parameter uncertainty. By Eq. 11, it approximates the sum of structural and experimental uncertainties. We can see these plots have different highlights, e.g., the white dot at the lower left.

## 5. Conclusions

In this work, we introduced an uncertainty quantification method based on the bias-variance decomposition. We showed how to apply this method to deep ensembles, and how to extract parameter uncertainty as well as experimental uncertainty (if the bias can be made small). The proposed two-stage procedure where we first fit a prediction model and then a separate model to predict the total uncertainty of this predictor leads to significant reduction in bias and better uncertainty prediction.

Our method shows strong adaptability to different models, is easy to implement and requires no modification to the prediction model. Lastly, we believe that we clarified some uncertainty quantification terminologies used in the existing papers and possible some misconceptions about epistemic uncertainty. For future work, we would like to further improve our method by taking into the account the parameter uncertainty in our prediction uncertainty network  $U$ , possible by also representing that with an ensemble. In addition, we like to apply these ideas to classification tasks.

## Acknowledgements

We thank Daniel Worrall, Patrick Forré, Tim Bakker, Balaji Lakshminarayanan, Yarin Gal and Alex Kendall for helpful discussions. This research was supported by NWO Perspective Grant DLMedIA as well as the in-cash and in-kind contributions by Philips.

## References

- Esteva, A., Kuprel, B., Novoa, R. A., Ko, J., Swetter, S. M., Blau, H. M., and Thrun, S. Dermatologist-level classification of skin cancer with deep neural networks. *Nature*, 2017.
- Gal, Y. and Ghahramani, Z. Dropout as a bayesian approximation: representing model uncertainty in deep learning. *ICML*, 2016.
- Goodfellow, I. J., Shlens, J., and Szegedy, C. Explaining and harnessing adversarial examples. *ICLR*, 2015.

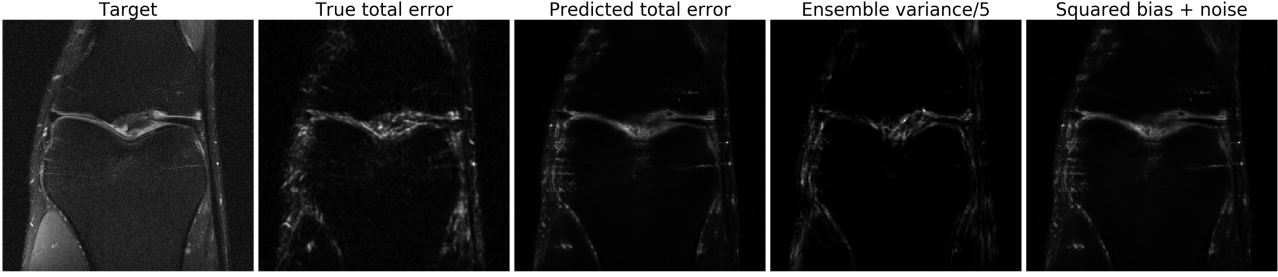


Figure 3. A random validation knee MRI, true and predicted total error, parameter uncertainty, squared bias + noise.

| Multi-coil U-net model applied to knee validation data           |                     |                         |                      |                         |
|--|---------------------|-------------------------|----------------------|-------------------------|
| Acceleration   | Method              | NMSE ↓                  | PSNR ↑               | SSIM ↑                  |
| 4-fold   | MC Dropout (p=0.1)  | 0.00933 ± 0.0061        | 36.41 ± 2.071        | 0.8910 ± 0.05652        |
|  | MC Dropout (p=0.2)  | 0.01027 ± 0.0055        | 35.91 ± 1.994        | 0.8852 ± 0.05570        |
|  | Ours + distillation | <b>0.00923</b> ± 0.0058 | <b>36.44</b> ± 2.055 | <b>0.8911</b> ± 0.05657 |
|  | Deep Ensemble       | 0.00823 ± 0.0059        | <b>37.07</b> ± 2.204 | <b>0.8982</b> ± 0.05774 |
|  | Deep Ensemble + AT  | 0.00836 ± 0.0059        | 36.98 ± 2.169        | 0.8976 ± 0.05760        |
|  | Ours                | <b>0.00823</b> ± 0.0057 | 37.05 ± 2.184        | 0.8976 ± 0.05728        |
| 8-fold   | MC Dropout (p=0.1)  | <b>0.01704</b> ± 0.0081 | <b>33.61</b> ± 1.920 | <b>0.8508</b> ± 0.05997 |
|  | MC Dropout (p=0.2)  | 0.01970 ± 0.0074        | 32.91 ± 1.912        | 0.8406 ± 0.05852        |
|  | Ours + distillation | 0.01717 ± 0.0068        | 33.53 ± 1.896        | 0.8503 ± 0.05972        |
|  | Deep Ensemble       | 0.01473 ± 0.0071        | 34.29 ± 1.943        | <b>0.8616</b> ± 0.06161 |
|  | Deep Ensemble + AT  | 0.01497 ± 0.0072        | 34.21 ± 1.932        | 0.8606 ± 0.06124        |
|  | Ours                | <b>0.01463</b> ± 0.0068 | <b>34.31</b> ± 1.925 | 0.8611 ± 0.06115        |
| Multi-coil Adaptive-CS-Net model applied to knee validation data |                     |                         |                      |                         |
| Acceleration   | Method              | NMSE ↓                  | PSNR ↑               | SSIM ↑                  |
| 4-fold   | Ours + distillation | 0.005883 ± 0.005324     | 39.17 ± 3.111        | 0.9149 ± 0.06344        |
|  | Ours                | 0.005776 ± 0.005036     | 39.25 ± 3.119        | 0.9155 ± 0.06341        |
| 8-fold   | Ours + distillation | 0.009856 ± 0.006105     | 36.29 ± 2.304        | 0.8852 ± 0.06586        |
|  | Ours                | 0.009623 ± 0.006418     | 36.44 ± 2.340        | 0.8868 ± 0.06578        |
| Multi-coil U-net model applied to FLAIR brain validation data    |                     |                         |                      |                         |
| Acceleration   | Method              | NMSE ↓                  | PSNR ↑               | SSIM ↑                  |
| 4-fold   | MC Dropout (p=0.1)  | 0.1491 ± 0.3822         | 32.58 ± 6.950        | 0.8124 ± 0.2226         |
|  | MC Dropout (p=0.2)  | <b>0.1464</b> ± 0.3712  | 32.23 ± 6.771        | 0.8091 ± 0.2199         |
|  | Ours + distillation | 0.1483 ± 0.3830         | <b>32.77</b> ± 7.022 | <b>0.8140</b> ± 0.2234  |
|  | Deep Ensemble       | 0.1489 ± 0.3826         | 32.58 ± 6.951        | 0.8182 ± 0.2258         |
|  | Deep Ensemble + AT  | 0.1480 ± 0.3842         | 33.14 ± 7.165        | 0.8180 ± 0.2255         |
|  | Ours                | <b>0.1470</b> ± 0.3819  | <b>33.19</b> ± 7.176 | <b>0.8185</b> ± 0.2248  |
| 8-fold   | MC Dropout (p=0.1)  | <b>0.1554</b> ± 0.3642  | 29.82 ± 5.903        | 0.7752 ± 0.2055         |
|  | MC Dropout (p=0.2)  | <b>0.1554</b> ± 0.3566  | 29.44 ± 5.732        | 0.7692 ± 0.2027         |
|  | Ours + distillation | 0.1570 ± 0.3737         | <b>30.01</b> ± 5.994 | <b>0.7779</b> ± 0.2074  |
|  | Deep Ensemble       | 0.1554 ± 0.3700         | 30.12 ± 6.029        | 0.7833 ± 0.2108         |
|  | Deep Ensemble + AT  | 0.1558 ± 0.3747         | 30.35 ± 6.121        | 0.7824 ± 0.2102         |
|  | Ours                | <b>0.1542</b> ± 0.3715  | <b>30.42</b> ± 6.140 | <b>0.7843</b> ± 0.2093  |

Table 3. Reconstruction prediction results on the validation set for the knee and FLAIR brain multi-coil tasks. The best mean predictions are in bold.

| Multi-coil U-net model applied to knee validation data           |                       |   |  |  |
|--|-----------------------|---|--|--|
| Acceleration   | Method                | $\mathcal{L}_1 (\times 10^{-6}) \downarrow$ | MSE ( $\times 10^{-11}$ ) $\downarrow$ | NMSE $\downarrow$                      |
| 4-fold   | MC Dropout (p=0.1)    | $2.679 \pm 1.461$                           | $2.275 \pm 2.796$                      | $0.5754 \pm 0.05061$                   |
|  | MC Dropout (p=0.2)    | $2.773 \pm 1.550$                           | $2.469 \pm 3.073$                      | $0.5617 \pm 0.04864$                   |
|  | Ours + distillation   | <b><math>2.302 \pm 1.221</math></b>         | <b><math>1.571 \pm 1.973</math></b>    | <b><math>0.3845 \pm 0.02686</math></b> |
|  | Deep Ensemble         | <b><math>2.123 \pm 1.094</math></b>         | $1.723 \pm 2.265$                      | $0.4783 \pm 0.06500$                   |
|  | Deep Ensemble + AT    | $2.550 \pm 1.295$                           | $2.461 \pm 3.069$                      | $0.6871 \pm 0.04953$                   |
|  | Ours                  | $2.143 \pm 1.084$                           | <b><math>1.338 \pm 1.672</math></b>    | <b><math>0.3950 \pm 0.03232</math></b> |
| 8-fold   | MC Dropout (p=0.1)    | $3.574 \pm 2.278$                           | $4.580 \pm 6.123$                      | $0.5248 \pm 0.03943$                   |
|  | MC Dropout (p=0.2)    | $3.956 \pm 2.596$                           | $5.727 \pm 7.579$                      | $0.5240 \pm 0.03591$                   |
|  | Ours + distillation   | <b><math>3.142 \pm 1.888</math></b>         | <b><math>3.843 \pm 5.081</math></b>    | <b><math>0.4161 \pm 0.02664</math></b> |
|  | Deep Ensemble         | <b><math>2.885 \pm 1.662</math></b>         | $3.267 \pm 4.409$                      | $0.4332 \pm 0.03759$                   |
|  | Deep Ensemble + AT    | $3.118 \pm 1.827$                           | $4.693 \pm 6.391$                      | $0.5917 \pm 0.05982$                   |
|  | Ours                  | $2.916 \pm 1.681$                           | <b><math>3.206 \pm 4.233</math></b>    | <b><math>0.4292 \pm 0.03220</math></b> |
| Multi-coil Adaptive-CS-Net model applied to knee validation data |                       |   |  |  |
| Acceleration   | Method                | $\mathcal{L}_1 (\times 10^{-6}) \downarrow$ | MSE ( $\times 10^{-11}$ ) $\downarrow$ | NMSE $\downarrow$                      |
| 4-fold   | Ours-U + distillation | $1.753 \pm 0.779$                           | $0.726 \pm 1.233$                      | $0.4025 \pm 0.03131$                   |
|  | Ours-A + distillation | <b><math>1.706 \pm 0.746</math></b>         | <b><math>0.684 \pm 1.298</math></b>    | <b><math>0.3749 \pm 0.02108</math></b> |
|  | Ours-U                | $1.754 \pm 0.784$                           | $0.727 \pm 1.231$                      | $0.4026 \pm 0.03207$                   |
|  | Ours-A                | <b><math>1.692 \pm 0.713</math></b>         | <b><math>0.655 \pm 1.145</math></b>    | <b><math>0.3747 \pm 0.01870</math></b> |
| 8-fold   | Ours-U + distillation | $2.486 \pm 1.328$                           | $1.727 \pm 2.347$                      | $0.4193 \pm 0.03072$                   |
|  | Ours-A + distillation | <b><math>2.332 \pm 1.199</math></b>         | <b><math>1.614 \pm 2.277</math></b>    | <b><math>0.3912 \pm 0.02321</math></b> |
|  | Ours-U                | $2.428 \pm 1.274$                           | $1.720 \pm 2.295$                      | $0.4215 \pm 0.03002$                   |
|  | Ours-A                | <b><math>2.302 \pm 1.172</math></b>         | <b><math>1.529 \pm 2.193</math></b>    | <b><math>0.3894 \pm 0.02590</math></b> |
| Multi-coil U-net model applied to FLAIR brain validation data    |                       |   |  |  |
| Acceleration   | Method                | $\mathcal{L}_1 (\times 10^{-5}) \downarrow$ | MSE ( $\times 10^{-9}$ ) $\downarrow$  | NMSE $\downarrow$                      |
| 4-fold   | MC Dropout (p=0.1)    | $1.277 \pm 2.330$                           | <b><math>1.146 \pm 3.164</math></b>    | $0.6476 \pm 0.1593$                    |
|  | MC Dropout (p=0.2)    | $1.342 \pm 2.376$                           | $1.204 \pm 3.160$                      | $0.6425 \pm 0.1617$                    |
|  | Ours + distillation   | <b><math>1.228 \pm 2.527</math></b>         | $1.278 \pm 3.562$                      | <b><math>0.4283 \pm 0.1505</math></b>  |
|  | Deep Ensemble         | $1.334 \pm 2.719$                           | $1.464 \pm 3.890$                      | $0.5907 \pm 0.1187$                    |
|  | Deep Ensemble + AT    | $1.311 \pm 2.459$                           | <b><math>1.275 \pm 3.399</math></b>    | $0.5804 \pm 0.0985$                    |
|  | Ours                  | <b><math>1.229 \pm 2.562</math></b>         | $1.298 \pm 3.614$                      | <b><math>0.4393 \pm 0.1536</math></b>  |
| 8-fold   | MC Dropout (p=0.1)    | $1.371 \pm 2.242$                           | $1.125 \pm 2.949$                      | $0.5562 \pm 0.1002$                    |
|  | MC Dropout (p=0.2)    | $1.411 \pm 2.211$                           | <b><math>1.124 \pm 2.836</math></b>    | $0.5589 \pm 0.1059$                    |
|  | Ours + distillation   | <b><math>1.278 \pm 2.370</math></b>         | $1.207 \pm 3.278$                      | <b><math>0.4299 \pm 0.1309</math></b>  |
|  | Deep Ensemble         | $1.348 \pm 2.500$                           | $1.340 \pm 3.456$                      | $0.5731 \pm 0.0979$                    |
|  | Deep Ensemble + AT    | <b><math>1.255 \pm 2.174</math></b>         | <b><math>1.066 \pm 2.888</math></b>    | $0.4846 \pm 0.0846$                    |
|  | Ours                  | $1.276 \pm 2.405$                           | $1.222 \pm 3.313$                      | <b><math>0.4455 \pm 0.1331</math></b>  |

Table 4. Uncertainty prediction results on the validation set for the knee and FLAIR brain multi-coil tasks. The best mean predictions are in bold. “Ours-U” or “Ours-A” means we use U-net or Adaptive-CS-Net to predict the errors of Adaptive-CS-Net.

Hinton, G., Vinyals, O., and Dean, J. Distilling the knowledge in a neural network. *arXiv 1503.02531*, 2015.

Hu, S., Worrall, D., Knecht, S., Veeling, B., Huisman, H., and Welling, M. Supervised uncertainty quantification for segmentation with multiple annotations. *MICCAI*, 2019.

Kendall, A. and Gal, Y. What uncertainties do we need in bayesian deep learning for computer vision? *NIPS*, 2017.

Kennedy, M. C. and O’Hagan, A. Bayesian calibration of

computer models. *Journal of the Royal Statistical Society*, 2001.

Kingma, D. P. and Ba, J. Adam: A method for stochastic optimization. *ICLR*, 2015.

Kiureghian, A. D. and Ditlevsen, O. Aleatory or epistemic? does it matter? *Special Workshop on Risk Acceptance and Risk Communication*, 2007.

Kohl, S. A. A., Romera-Paredes, B., Meyer, C., Fauw, J. D.,



- Ledsam, J. R., Maier-Hein, K. H., Eslami, S. M. A., Rezende, D. J., and Ronneberger, O. A probabilistic u-net for segmentation of ambiguous images. *NeurIPS*, 2018.
- Lakshminarayanan, B., Pritzel, A., and Blundell, C. Simple and scalable predictive uncertainty estimation using deep ensembles. *NIPS*, 2017.
- Nair, V. and Hinton, G. E. Rectified linear units improve restricted boltzmann machines. *ICML*, 2010.
- Nix, D. A. and Weigend, A. S. Estimating the mean and variance of the target probability distribution. *IEEE International Conference on Neural Networks*, 1994.
- Pezzotti, N., de Weerd, E., Yousefi, S., Elmahdy, M. S., van Gemert, J., Schlke, C., Doneva, M., Nielsen, T., Kastrup, S., Lelieveldt, B. P., van Osch, M. J., and Staring, M. Adaptive-cs-net: Fastmri with adaptive intelligence. *arXiv preprint arXiv:1912.12259*, 2019.
- Rajpurkar, P., Irvin, J., Zhu, K., Yang, B., Mehta, H., Tony Duan, D. D., Bagul, A., Langlotz, C., Shpanskaya, K., Lungren, M. P., and Ng, A. Y. Chexnet: Radiologist-level pneumonia detection on chest x-rays with deep learning. *arXiv preprint arXiv:1711.05225*, 2017.
- Ronneberger, O., Fischer, P., and Brox, T. U-net: Convolutional networks for biomedical image segmentation. *MICCAI*, 2015.
- Srivastava, N., Hinton, G., Krizhevsky, A., Sutskever, I., and Salakhutdinov, R. Dropout: A simple way to prevent neural networks from overfitting. *JMLR*, 2014.
- Tanno, R., Worrall, D. E., Ghosh, A., Kaden, E., Sotiropoulos, S. N., Criminisi, A., and Alexander, D. C. Bayesian image quality transfer with cnns: Exploring uncertainty in dmri super-resolution. *MICCAI*, 2017.
- Tieleman, T. and Hinton, G. Lecture 6.5 - rmsprop: Divide the gradient by a running average of its recent magnitude. COURSE: Neural networks for machine learning, 2012.
- Witherspoon, S. and Fadrhonic, W. Machine learning can boost the value of wind energy. <https://blog.google/technology/ai/machine-learning-can-boost-value-wind-energy/>, 2019.
- Zbontar, J., Knoll, F., Sriram, A., Muckley, M. J., Bruno, M., Defazio, A., Parente, M., Geras, K. J., Katsnelson, J., Chandarana, H., Zhang, Z., Drozdal, M., Romero, A., Rabbat, M., Vincent, P., Pinkerton, J., Wang, D., Yakubova, N., Owens, E., Zitnick, C. L., Recht, M. P., Sodickson, D. K., and Lui, Y. W. fastmri: An open dataset and benchmarks for accelerated mri. *arXiv 1811.08839*, 2018.
- Zhu, L. and Laptev, N. Deep and confident prediction for time series at uber. *IEEE International Conference on Data Mining Workshops (ICDMW)*, 2017.